GIANT PULSES — THE MAIN COMPONENT OF THE RADIO EMISSION OF THE CRAB PULSAR

M. V. Popov,[1] V. A. Soglasnov,[1] V. I. Kondrat'ev,[1]
S. V. Kostyuk,[1] Yu. P. Ilyasov,[2] and V. V. Oreshko[2]

[1] *Astro Space Center, Lebedev Physical Institute, Moscow, Russia*

[2] *Pushchino Radio Astronomy Observatory, Astro Space Center, Lebedev Physical Institute, Pushchino, Russia*

(Received May 20, 2005; Revised July 6, 2005)

The paper presents an analysis of dual-polarization observations of the Crab pulsar obtained on the 64-m Kalyazin radio telescope at 600 MHz with a time resolution of 250 ns. A lower limit for the intensities of giant pulses is estimated by assuming that the pulsar radio emission in the main pulse and interpulse consists entirely of giant radio pulses; this yields estimates of 100 Jy and 35 Jy for the peak flux densities of giant pulses arising in the main pulse and interpulse, respectively. This assumes that the normal radio emission of the pulse occurs in the precursor pulse. In this case, the longitudes of the giant radio pulses relative to the profile of the normal radio emission turn out to be the same for the Crab pulsar and the millisecond pulsar B1937+21, namely, the giant pulses arise at the trailing edge of the profile of the normal radio emission. Analysis of the distribution of the degree of circular polarization for the giant pulses suggests that they can consist of a random mixture of nanopulses with 100% circular polarization of either sign, with, on average, hundreds of such nanopulses within a single giant pulse.

1. INTRODUCTION

Giant pulses are short-time-scale flares of radio emission whose peak flux densities exceed the peak flux density in the mean pulse profile of the pulsar by a factor of hundreds or thousands. Although there have recently been a number of publications reporting the detection of strong, brief pulses in several pulsars [1–5], detailed studies of the properties of giant radio pulses have been presented for only two pulsars: the Crab pulsar (B0531+21;

see references in [6, 7]) and the millisecond pulsar B1937+21 [8–12].

2. OBSERVATIONS AND REDUCTION

The observations considered here were carried out on November 25–26, 2003 at 600 MHz on the 64-m Kalyazin radio telescope. The duration of the observing session processed was three hours. The observations were obtained in the framework of an international program of multi-frequency studies of the properties of the Crab pulsar's giant pulses. Other telescopes participating in this program include the 100-m Effelsberg radio telescope (8350 MHz), 76-m Lovell Telescope at Jodrell Bank (1400 MHz), the Westerbork Radio Synthesis Telescope (1200 MHz), the Large Phased Array and DKR-1000 radio telescope of the Pushchino Radio Astronomy Observatory (111 MHz), and the T-shaped UTR-2 radio telescope in Khar'kov (23 MHz). In addition, simultaneous optical observations were obtained on the 6-m telescope of the Special Astrophysical Observatory and the 2.9-m telescope at La Palma. The MAGIC and HESS gamma-ray telescopes in La Palma and Namibia, which detect Cerenkov radiation in the upper layers of the atmosphere due to the passage of high-energy gamma-rays, also participated. We present here only an analysis of the Kalyazin observations at 600 MHz. A joint analysis of the multi-frequency observations will be presented in other publications.

The Kalyazin radio telescope received radio emission in two channels, sensitive to left- and right-circular polarization (LCP and RCP). Each polarization channel recorded two frequency bands (upper and lower sideband), each with a width of 4 MHz, with the central frequency being 600.0 MHz. Thus, the time resolution of the observations was 250 ns. The data were recorded on a video cassette with two-bit sampling using an S2 recording system. The data were played back after the observations at the Astro Space Center of the Lebedev Physical Institute using the specialized S2-RDR system developed in the Astrophysical Data-Reduction Department of the Astro Space Center. We removed the influence of the dispersion of the radio waves using the method of pre-detection dispersion compensation [13]. The reduction methods used are described in [14]. The procedure used to reconstruct the signal is very computer-intensive: 10 minutes of observational data were processed in 20 hours. When reconstructing the signal, we used the emission measure of 56.757, taken from the monthly ephemerides of the Jodrell Bank Observatory [15].

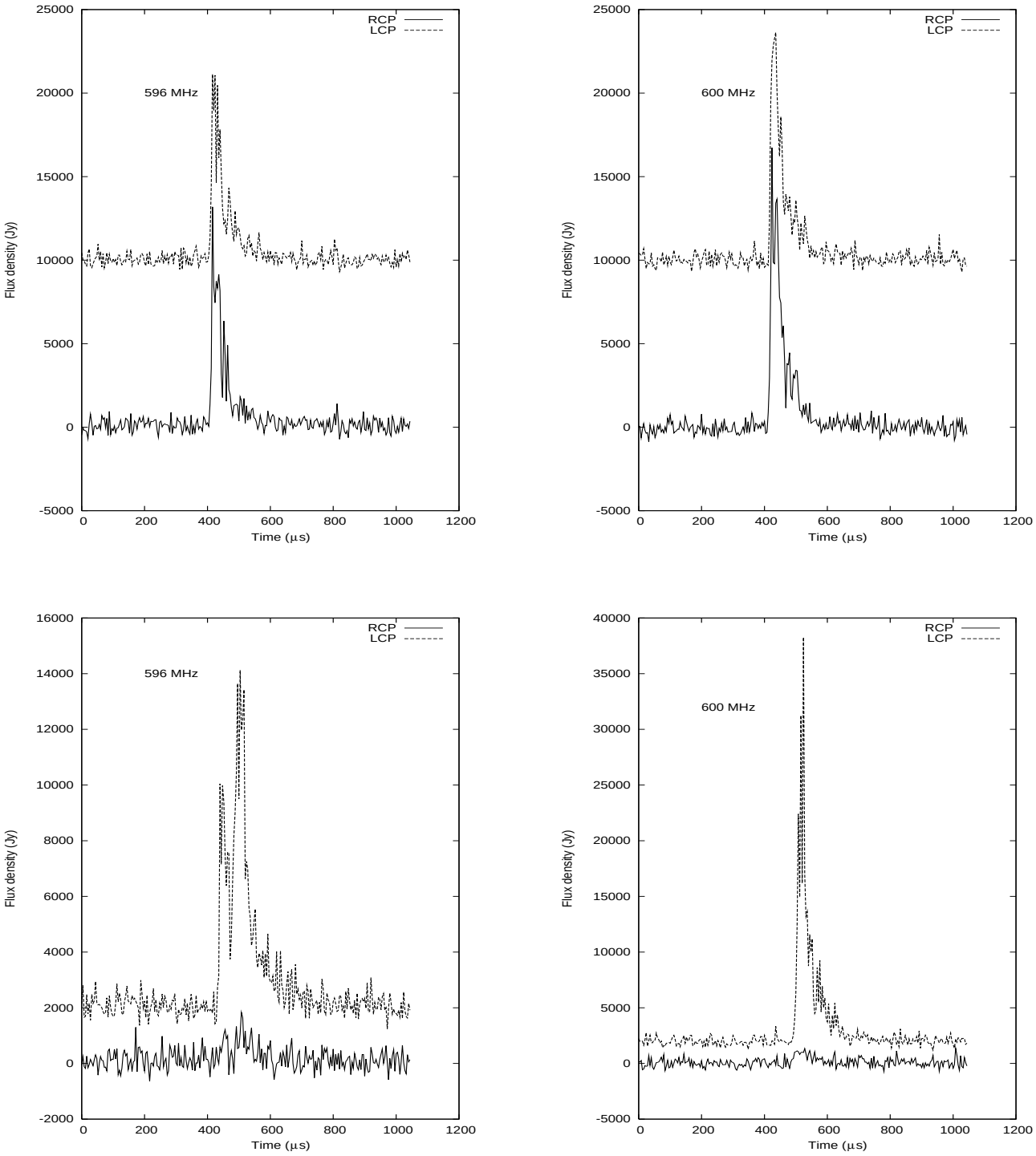

Figure 1. Two strong giant pulses after averaging to 8 ms. The dashed and solid curves show the signals in left- and right-circular polarization, respectively. The observed shape of the pulses is due to scattering of the radio waves on inhomogeneities in the interstellar plasma.

3. DETECTION CRITERIA

Broadening of the pulse due to dispersion in the interstellar plasma (by about 8.5 ms in our case) was fully corrected for using the method of pre-detection dispersion compensation. However, scattering on inhomogeneities in the interstellar plasma also significantly broadens the pulse. As we will show in Section 4, the effective width of the pulse due to scattering was 60 μs for our session. Therefore, to increase the sensitivity of the search for giant pulses, we averaged the reconstructed signal over 32 μs (256 points). Since it is well known that giant radio pulses from the Crab pulsar are observed only in narrow longitude intervals corresponding to the positions of the main pulse and interpulse, we searched for radio flares only in these two longitude "windows," synchronized with the pulsar period. The width of each window was 960 μs, or 30 points of the averaged recording. Events were taken to represent giant pulses if the amplitude of the signal in one of the windows exceeded $5\,\sigma$ relative to the mean level in at least one of the four channels. We also required that the amplitude at that same point in one of the three remaining channels (allowing for the dispersion delay between channels) exceeded $3.5\,\sigma$. After averaging over 256 points, the distribution of signal amplitudes was close to a normal distribution, for which the probabilities of exceeding the $5\,\sigma$ and $3.5\,\sigma$ levels are 2.87×10^{-7} and 2.32×10^{-4}, respectively. The total probability of a random realization of our detection criteria is then 8×10^{-10}. In each pulsar period, 60 measurements are made, and 2×10^7 are made over three hours of observations, so that the expected number of false giant pulses is only 0.015. Thus, all the detected giant pulses are real. Over the three hours of observations, we detected 4287 giant pulses, of which 3802 were at the longitudes of the main pulse and 485 at the longitudes of the interpulse.

Figure 1 shows examples of strong giant pulses. The flux-density scale is established in accordance with the rms deviation, which is 1270 Jy, and is determined primarily by the contribution of the radio emission of the Crab nebula. The basis for this estimation is given in [16]. For our subsequent analysis, we must know the effective threshold peak flux density of the giant pulses detected according to the described criteria. This value was determined from the distribution of the peak flux densities of the detected giant pulses shown in Fig. 2. The peak flux density was determined by averaging over all frequencies and polarizations. The distribution in Fig. 2 shows a sharp cutoff at a flux density of about 300 Jy, and this value was adopted for the minimum peak flux density for the giant pulses detected in our

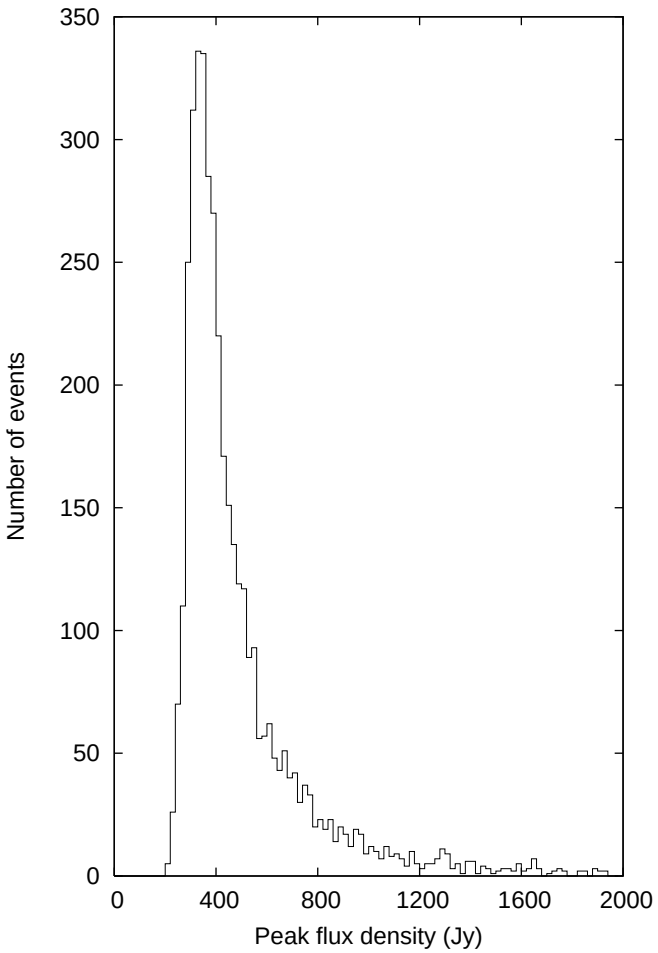

Figure 2. Distribution of the peak flux densities of the detected giant pulses.

analysis.

4. SCATTERING PROFILE

The shape of the detected giant radio pulses is fully determined by scattering on inhomogeneities of the interstellar plasma, as we can clearly see in Fig. 1. The giant pulses have a steep front and an exponential tail. To determine the effective widths of the giant pulses, we constructed a mean giant-pulse profile by averaging all the detected pulses with peak flux densities greater than 800 Jy. During the averaging, the pulses were equalized according to the point at the leading front, for which the amplitude of the deviation from the mean value outside the pulse was less than 30% of the maximum amplitude of the given pulse (this equalization was carried out for the signal averaged over a time of 8μs). The resulting mean giant-pulse profile is shown in the right-hand part of Fig. 3. The left-hand part of this figure

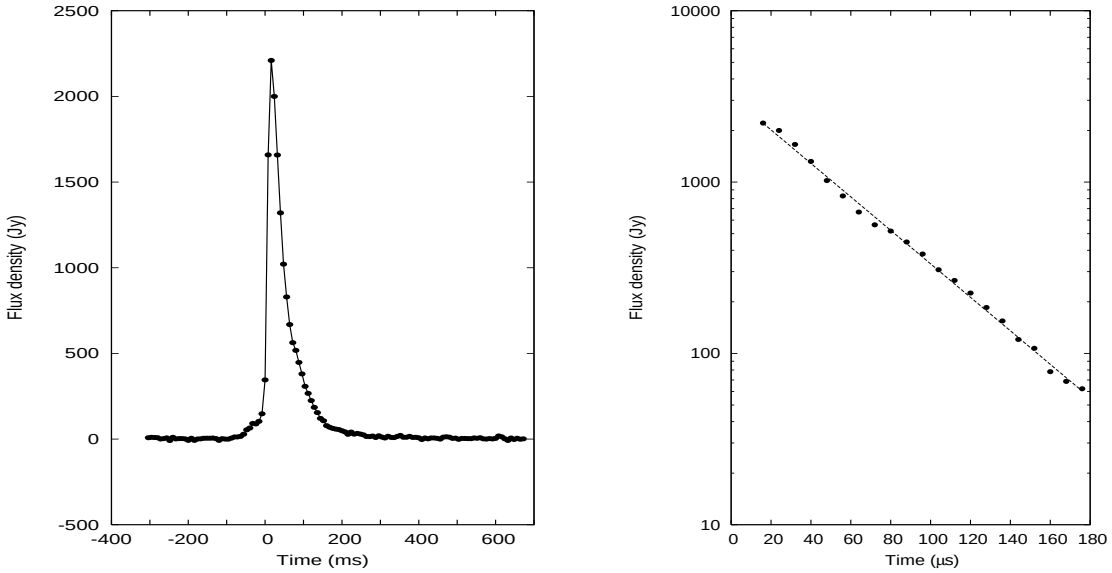

Figure 3. The scattering profile of the giant pulses (left) and an exponential approximation to the tail of the profile (right). The exponential time constant is 45 μs.

shows the time dependence of the intensity for the trailing edge of the pulse on a half-log scale. We can see that the observed points are approximated well by a linear dependence, and that the shape of this part of the profile corresponds to an exponential decay, $S = S_p e^{-t/\tau}$, with the characteristic time $\tau = 45 \pm 5$ μs. Taking into account the leading front of the pulse, we adopted for the effective width of the giant-pulse profile $W_e = 60$ μs. This width was used to calculate the energy of the detected giant pulses $E = S_p W_e$, where S_p is the peak flux density.

5. ENERGY DISTRIBUTION

Figure 4 shows the distributions of the integrated energy of the detected giant pulses separately for pulses at the longitudes of the main pulse and interpulse. Near the mean energies, both distributions are approximated well by power laws, $N(E) \propto E^{-\alpha}$, with the same index, $\alpha = 2.20 \pm 0.06$. Deviations from this behavior at small energies are due to the incompleteness of the pulse detection, while deviations at large energies are due to insufficient statistics. The most representative studies of the statistics of giant pulses from the Crab pulsar are those of Lundgren et al. [17], who detected about 30 000 giant pulses over several

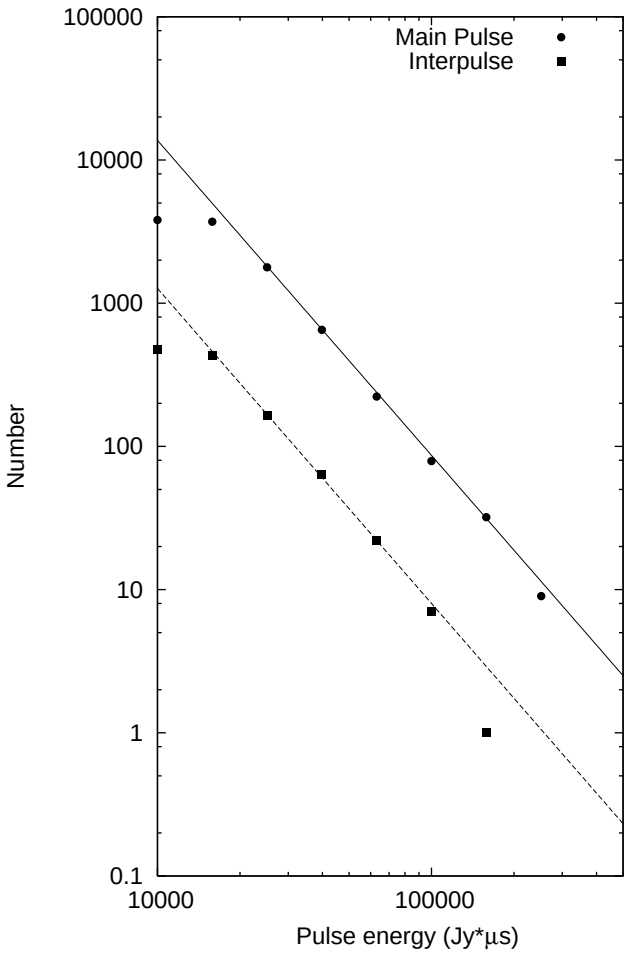

Figure 4. Integrated energy distribution of the giant pulses. The circles and squares show data for giant pulses detected at the longitudes of the main pulse and interpulse, respectively. The straight lines correspond to a power law with index -2.2.

days of observations with the 43-m Green Bank radio telescope at 800 MHz. The values of the index α they derived were different on different days, and were contained in the interval 3.06–3.36. Cordes et al. [18] obtained the index $\alpha = 2.3$ for the distribution of the peak flux densities of giant pulses observed at 430 MHz, which is much closer to our value derived at 600 MHz.

6. GIANT PULSES AND THE MEAN PROFILE OF THE PULSAR

Figure 5 compares the mean profiles of B0531+21 obtained by averaging all the pulses detected over the observation period ($N = 320\,913$) and averaging only the detected giant

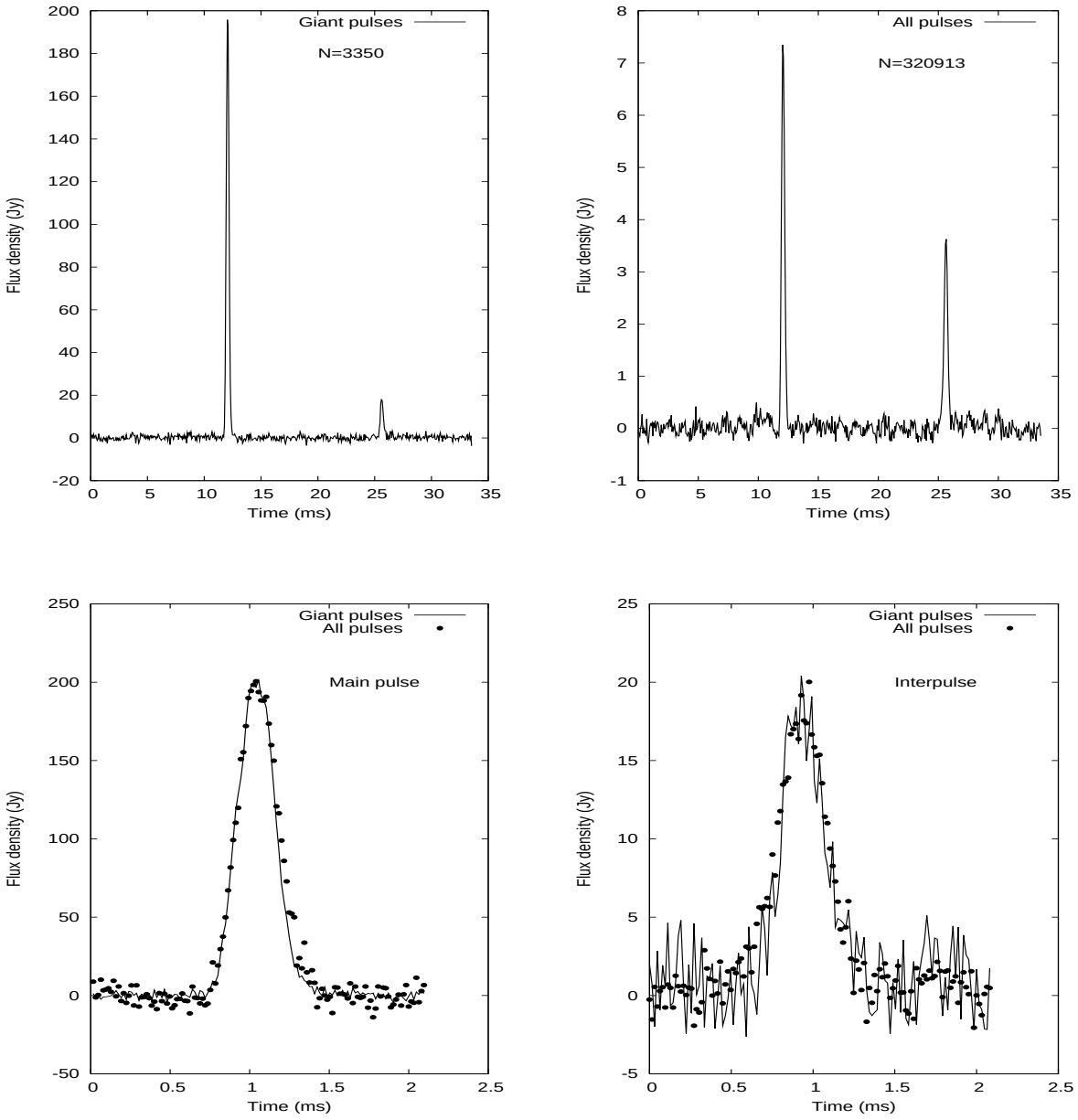

Figure 5. Upper plots: mean profiles obtained by averaging 3350 giant pulses (left) and by averaging all 320 913 pulses (right). Lower plots: comparison of the profile shapes after the mean profiles have been scaled to have the same amplitude.

pulses ($N = 3350$). We can clearly see that the mean profile for the giant pulses has a higher signal-to-noise ratio, although the total profile includes a hundred times as many individual pulses. This same conclusion was reached by Cordes et al. [18]. Moreover, the shapes of the two profiles (lower part of Fig. 5) are surprisingly similar, as was earlier pointed out by

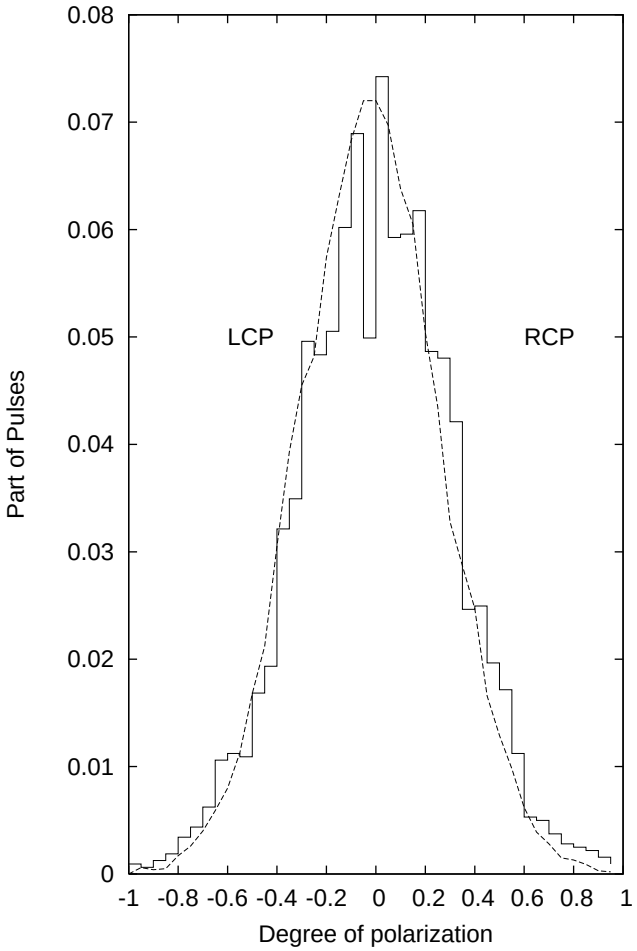

Figure 6. Distribution of the degree of circular polarization for the giant pulses. The dashed curve shows the results of our simulations (see text for more information).

Friedman and Boriakoff [19]. All this suggests that the pulsar emission in the main pulse and interpulse consist entirely of giant radio pulses. We suggest that the "normal" radio emission of the pulsar is concentrated in the precursor pulse, which is barely distinguishable in our observations (upper right plot in Fig. 5). In this case, the longitudes of the giant pulses in the mean profile of B0531+21 become identical to the longitude distribution for the giant pulses of the millisecond pulsar B1937+21, for which all the giant pulses arise at the trailing edges of the main pulse and interpulse [8–10]. Friedman and Boriakoff [19] also suggest the possible presence of a precursor pulse near the interpulse of the Crab pulsar, providing additional evidence in support of our hypothesis.

Assuming that the radio emission in the main pulse and interpulse consists only of giant pulses and that the energy distribution of these pulses follows a power law with index -2.2

down to some lower limit, we can determine this limit by comparing the total energy in the detected giant pulses, which have a known detection limit, and the total energy in all the pulses observed in the session. This yields for the giant pulses at the longitudes of the main pulse and interpulse lower limits for the peak flux density of 105 Jy and 25 Jy, respectively. Let us now estimate the total number of potentially observable giant pulses at 600 MHz. If we change these estimates slightly to the values 100 and 35 Jy, which lie within their uncertainties, the total number of potentially observable giant pulses at the longitude of the main pulse and interpulse become the same, equal to 42 000 pulses over the three hours of observations, which corresponds to a mean rate of appearance of the giant pulses of four per second. Using the fact that the giant pulses can be observed only within narrow longitude intervals corresponding to the observed width of the profiles of the main pulse and interpulse (about 0.5 ms), we can estimate the total mean rate of appearance of giant pulses, which is approximately 270 pulses per second, or about 10 giant pulses per rotation of the neutron star, for the longitudes of both the main pulse and interpulse.

Lundgren et al. [17] estimated the minimum threshold peak flux density for the giant pulses from B0531+21, obtaining about 50 Jy at 800 MHz without distinguishing between giant pulses corresponding to the main pulse and interpulse. They assumed the presence of weak, continuously arising micropulses with flux densities of 1–2 Jy in addition to the giant pulses. We cannot refute this suggestion, but consider it to be unnecessary.

7. POLARIZATION OF THE GIANT PULSES

The two giant pulses presented in Fig. 1 as examples display completely different polarization characteristics: the pulse in the upper plots has equal intensities in RCP and LCP, while the pulse in the lower plots is almost 100% left-circularly polarized. Little has been published about the polarization properties of individual giant pulses. In their study of giant pulses from the millisecond pulsar B1937+21, Cognard et al. [8] show that giant pulses with high degrees of either LCP or RCP frequently appear. Popov et al. [11] also reported the detection of giant pulses from B1937+21 with high degrees of circular polarization of both signs at 600 MHz. Hankins et al. [7] showed that nanopulses detected in the structure of giant pulses from B0531+21 have high degrees of circular polarization, with individual nanopulses separated in time by several microseconds sometimes displaying opposite signs

of circular polarization.

Returning to our 600-MHz observations, we note that the pulse with strong circular polarization shown in Fig. 1 is the only such example among the strong giant pulses. The solid step-wise line in Fig. 6 shows the observed distribution of the circular polarization for all detected giant pulses with peak flux densities exceeding 500 Jy. We calculated the degree of polarization as $\frac{R-L}{R+L}$, where R and L are the peak flux densities in RCP and LCP averaged over the two frequency channels. We can see from Fig. 6 that pulses with high degrees of polarization are not rare, although the vast majority of the pulses have degrees of polarization in the range $-0.4 \ldots +0.4$.

Based on the results of Hankins et al. [7], we supposed that all giant pulses consist of nanopulses with 100% circular polarization of one or the other sign, and carried out numerical simulations of the expected circular-polarization distribution for events under this assumption. In the simulations, individual nanopulses were generated as the sum of the squares of two components, which we arbitrarily call the real and imaginary components of the nanopulse. The components were taken from a normal distribution with a zero mean and unit dispersion. The sign of the polarization of the nanopulse was determined by the sign of the imaginary component. The amplitude distribution for the generated nanopulses corresponds to a χ^2 distribution with two degrees of freedom, as should be the case for a detected signal without averaging. For each simulated giant pulse, we specified the number of constituent nanopulses, again calculating the degree of polarization as $\frac{R-L}{R+L}$, where R and L are the sums of the amplitudes of the nanopulses with RCP (a positive imaginary component) and LCP (a negative imaginary component), respectively. The simulations were carried out for various numbers of constituent nanopulses from 10 to 1000. We ran 10 000 trials in order to construct the distribution. The dashed line in Fig. 6 shows the simulated distribution for the case of 100 nanopulses making up each giant pulse, which is the model distribution that best agrees with the observed distribution.

8. DISCUSSION

Our suggestion that the radio emission of the Crab pulsar at the longitudes of the main pulse and interpulse consists entirely of giant radio pulses removes one substantial difference between the properties of the giant pulses of the Crab pulsar and the millisecond pulsar

B1937+21. It was immediately noted for the latter pulsar that the giant pulses arise outside the mean profile for the normal radio emission, at the trailing edges of the profiles of the main pulse and interpulse [9, 10]. We propose that the normal radio emission of the Crab pulsar is generated at the longitudes of the precursor pulse preceeding the main pulse and interpulse, so that the giant pulses making up these components are localized at the trailing edges of the profiles corresponding to the normal radio emission, as in the case of the millisecond pulsar B1937+21. This unification of the properties of the giant radio pulses of these two pulsars could be very important for our understanding of the origin of the giant pulses.

Another appreciable difference in the parameters of the giant pulses observed from the millisecond pulsar B1937+21 and the Crab pulsar is their characteristic duration. The analysis of Hankins [20], carried out at 4.9 GHz, where scattering on inhomogeneities in the interstellar plasma does not appreciably affect the pulse profile, shows that the intrinsic durations of the giant pulses from the Crab pulsar are typically several microseconds. The giant pulses from B1937+21 have been unresolved in all published studies. Soglasnov et al. [10] showed that the intrinsic durations of the giant pulses from this pulsar are less than 15 ns. However, Hankins et al. [7] showed that the giant pulses generated by the Crab pulsar include some that consist entirely of unresolved nanopulses with durations of less than 2 ns, with these nanopulses often displaying 100% circular polarization. Our analysis in Section 7 indicates that the circular-polarization distribution for the giant pulses is consistent with the hypothesis that these pulses consist of, on average, hundreds of nanopulses, each with 100% LCP or RCP. Thus, the difference in the durations of the giant radio pulses from the millisecond pulsar and the Crab pulsar is not important. Namely, this difference corresponds only to differences in the number of nanopulses comprising each giant pulse: no more than a few dozen in the case of the millisecond pulsar and, on average, hundreds in the case of the Crab pulsar. We suggest that the nanopulses making up the giant pulses from the Crab pulsar and millisecond pulsar have the same nature.

9. ACKNOWLEDGMENTS

The authors thank K.G. Belousov and A.V. Chibisov for providing the operational S2-RDR play-back system. This work was supported by the Russian Foundation for Basic Research (project code 04-02-16384) and the basic research program of the Presidium of the

Russian Academy of Sciences on "Non-stationary Phenomena in Astronomy."

---

1. S. Johnston, W. van Straten, M. Kramer, *et al.*, Astrophys. J. **549**, 101 (2001).
2. M. Kramer, S. Johnston, and W. van Straten, Mon. Not. R. Astron. Soc. **334**, 523 (2002).
3. R. W. Romani and S. Johnston, Astrophys. J. **557**, 93 (2001).
4. S. Johnston and R. W. Romani, Mon. Not. R. Astron. Soc. **332**, 109 (2002).
5. A. A. Ershov and A. D. Kuz'min, Pis'ma Astron. Zh. **29**, 111 (2003) [Astron. Lett. **29**, 91 (2003)].
6. S. Sallmen, D. C. Backer, J. H. Taylor, *et al.*, Astrophys. J. **517**, 460 (1999).
7. T. H. Hankins, J. S. Kern, J. C. Weatherall, and J. A. Eilek, Nature **422**, 141 (2003).
8. I. Cognard, J. A. Shrauner, J. H. Taylor, and S. E. Thorsett, Astrophys. J. **457**, L81 (1996).
9. A. Kinkhabwala and S. E. Thorsett, Astrophys. J. **535**, 365 (2000).
10. V. A. Soglasnov, M. V. Popov, N. Bartel, *et al.*, Astrophys. J. **616**, 439 (2004).
11. S. V. Kostyuk, V. I. Kondrat'ev, A. D. Kuz'min, *et al.,* Pis'ma Astron. Zh. **29**, 440 (2003) [Astron. Lett. **29**, 387 (2003)].
12. M. V. Popov and B. Stappers, Astron. Zh. **80**, 717 (2003) [Astron. Rep. **47**, 660 (2003)].
13. T. H. Hankins, Astrophys. J. **158**, 487 (1971).
14. M. V. Popov, N. Bartel, W. Cannon, *et al.*, Astron. Astrophys. **396**, 171 (2002).
15. Jodrell Bank Crab Pulsar Monthly Ephemeris, `http://www.jb.man.ac.uk/~pulsar/crab.html`.
16. S. V. Kostyuk, V. I. Kondrat'ev, A. D. Kuz'min, *et al.,* Pis'ma Astron. Zh. **29**, 440 (2003) [Astron. Lett. **29**, 387 (2003)].
17. S. C. Lundgren, J. M. Cordes, M. Ulmer, *et al.*, Astrophys. J. **453**, 433 (1995).
18. J. M. Cordes, N. D. R. Bhat, T. H. Hankins, *et al.*, Astrophys. J. **612**, 375 (2004).
19. J. F. Friedman and V. Boriakoff, *IAU Coll. 128: The Magnetospheric Structure and Emission Mechanisms of Radio Pulsars,* Ed. by T. H. Hankins, J. M. Rankin, and J. A. Gil (Pedagogical Univ. Press, Poland, 1992), p. 347.
20. T. H. Hankins, *IAU Coll. 177: Pulsar Astronomy "— 2000 and Beyond,* Ed. by M. Kramer, N. Wex, and R. Wielebinski, Astron. Soc. Pac. Conf. Ser. **202**, 165 (2000).